RMetS
Royal Meteorological Society

Comparison of Lorenz and Charney–Phillips vertical discretisations for dynamics–boundary layer coupling. Part II: Transients

D. Holdaway,[a,b,c*] J. Thuburn[a] and N. Wood[d‡]

[a]*College of Engineering, Mathematics and Physical Sciences, University of Exeter, UK*
[b]*Goddard Earth Sciences Technology and Research, Universities Space Research Association, MD, USA*
[c]*Global Modeling and Assimilation Office, NASA Goddard Space Flight Center, MD, USA*
[d]*Met Office, Exeter, UK*

*Correspondence to: D Holdaway, Code 610.1, Goddard Space Flight Center, Greenbelt, MD 20771, USA.
E-mail: dan.holdaway@nasa.gov
‡The contribution of this author was written in the course of his employment at the Met Office, UK, and is published with the permission of the Controller of HMSO and the Queen's Printer for Scotland

A numerical comparison of the Lorenz and Charney–Phillips vertical grids for capturing the steady state of a set of equations that models the large-scale dynamics of the atmosphere and the planetary boundary layer (Part I of this article) has revealed important differences between the grids. Due to suppression of a negative feedback, Charney–Phillips grids that involve averaging of shear in the boundary-layer terms are not able to capture the structure of the boundary layer accurately. The Lorenz grid performs well in terms of capturing the boundary layer on its own, but the Charney–Phillips grids that use averaging of potential temperature gradient are generally preferred once dynamics are included. Any finite-difference approximation of the problem must be capable of accurately representing both the steady-state and time-dependent parts of the solution. In this Part II of the article, the ability of the Lorenz and Charney–Phillips configurations to capture the transient part of the system is considered. The configurations are compared in terms of their ability to capture the eigenmodes of the solution. Full comparison between Lorenz and Charney–Phillips grids is limited by non-normality of the linearised system, associated with the boundary layer. The Lorenz grid computational mode is examined. The structure is modified by the boundary layer but it still exists. For the modes that could be accurately examined, it is found that both grids perform well in terms of capturing spatial and temporal mode structure. Some Lorenz grid modes are identified that have spurious computational mode-like behaviour occurring near the top of the boundary layer. Copyright © 2012 Royal Meteorological Society

Key Words: physics–dynamics coupling; computational mode; eigenmodes; atmospheric waves

Received 27 March 2012; Revised 15 June 2012; Accepted 9 July 2012; Published online in Wiley Online Library 21 September 2012

Citation: Holdaway D, Thuburn J, Wood N. 2013. Comparison of Lorenz and Charney–Phillips vertical discretisations for dynamics–boundary layer coupling. Part II: Transients. *Q. J. R. Meteorol. Soc.* **139**: 1087–1098. DOI:10.1002/qj.2017

1. Introduction

The Lorenz (Lorenz, 1960) and Charney–Phillips (Charney and Phillips, 1953) vertical discretisations have been compared for their ability to capture the steady state of a set of equations that simultaneously represent the large-scale dynamics of the atmosphere and the planetary boundary layer (Holdaway *et al.*, 2012, hereafter Part I). From examining the steady states of this so-called physics–dynamics coupling problem, important differences between the ability of the two types of grid are found, namely:

- The Lorenz grid is preferred for modelling the steady-state boundary layer on its own.
- For the coupled steady state, the Charney–Phillips grids that use averaging of potential temperature gradient and either averaging of eddy diffusivity or Richardson number in the boundary-layer terms are preferred.
- Charney–Phillips configurations that involve averaging of shear behave poorly due to a suppression of a negative feedback, which leads to discontinuities in the vertical structure of the predicted fields.

Examining the steady states is useful for investigating general differences and ruling out problematic configurations. However, in order to gain a full understanding of the differences between the Lorenz and Charney–Phillips grids for the dynamics–boundary layer coupled problem it is necessary to also consider the time-dependent (transient) part of the linearisation. A convenient method for comparing the transients, and as used by Leslie and Purser (1992), Fox-Rabinovitz (1994), Thuburn and Woollings (2005) and Thuburn (2006) to compare vertical configurations, is to examine the eigenmodes.

Eigenmode analysis is a powerful technique since it allows one to examine the individual scales of motion supported by the problem and thus see for which scales and physical behaviour a particular configuration performs well. Further, it does not rely on constructing a set of initial conditions and thus offers very general results. A further advantage of the eigenmode approach is that it allows for explicit examination of how the Lorenz grid computational mode interacts with the boundary-layer diffusion.

An inviscid resting 'dynamics only' atmosphere supports three types of familiar dynamical modes: acoustic, inertio-gravity and Rossby. The behaviour of these dynamical modes is well described by Holton (2004). Acoustic and inertio-gravity modes occur in eastward- and westward-propagating pairs. One pair of acoustic modes and one Rossby mode are external; for a rigid lid boundary condition, inertio-gravity modes are all internal. It is important that a discrete model of the atmosphere stably captures the faster propagating acoustic and inertio-gravity modes so that it accurately represents adjustment to hydrostatic and geostrophic balance. It is important to capture the more slowly propagating Rossby modes accurately since they are energetically dominant and determine large-scale structures in the atmosphere.

When the atmospheric equations are discretised on the Lorenz grid, there exists one more degree of freedom than necessary for the number of physical modes, resulting in the associated computational mode. The extra degree of freedom is due to the placement of one of the thermodynamic variables relative to the boundaries. The additional averaging that results in the vertical momentum equation leads to the computational mode manifesting itself as a 'two-grid' wave in one or more of the thermodynamic prognostic variables, that is 'invisible' to the system (Arakawa and Konor, 1996; Kalnay, 2003; Thuburn and Woollings, 2005; Lauritzen *et al.*, 2011). The mode is non-physical, does not properly propagate and can interact nonlinearly with the other modes, creating overall inaccuracy.

The inclusion of a more complex sheared reference state and the boundary-layer diffusion will distort some of the dynamical modes and some will be replaced by boundary-layer modes, discussed in section 5.3. If the computational mode is distorted, or even replaced, by the inclusion of the boundary layer, then this could mitigate the problems that it can lead to and alleviate the main disadvantage of the Lorenz grid.

As described in section 5.1 of Part I, a model that captures just the stratified atmospheric boundary layer with minimal dynamics can be constructed (Stull, 1988; Garrett, 1992; Holton, 2004). A 'boundary layer only' model usually makes use of the Boussinesq approximation. Further it assumes no vertical wind and no horizontal advection, allowing horizontal pressure gradients to be replaced by the geostrophic balance value.

A boundary layer-only model will capture boundary-layer, or diffusive, modes. Boundary-layer modes have all their structure in the boundary-layer region and have varying decay rate that generally dominates the rate of propagation. It is important that a discrete model captures these modes accurately, since the boundary layer is responsible for a number of important temporal physical processes, such as the nocturnal jet, dispersion of aerosols, turbulence and Ekman pumping. The boundary layer-only model will also capture some undamped inertial modes that live above the boundary layer and propagate with the background flow. Whereas for the dynamics-only case it is possible to analytically describe each type of mode and their structure, this is not possible for a stratified boundary-layer model.

When the dynamics and boundary-layer components are coupled, the resulting problem is considerably more complex, in terms of both the reference state and the supported physical processes, than the problems for which eigenmode analysis has typically been used previously. The extra complexity makes the methodology and its interpretation considerably more difficult.

When written in an appropriate basis (energy variables—section 3.1 below) the inviscid resting reference state case of Thuburn and Woollings (2005) has orthogonal (i.e. normal) eigenvectors and the system matrix is said to be 'normal'. The choice of basis does not affect the physical structure of the eigenmodes, so the fact that the system is normal in an appropriate basis means that analysing eigenmodes, or normal modes, is straightforward. Individual normal modes can be interpreted physically and can be easily compared across varying configurations. However, when the background reference state has shear, or boundary layer terms are included, the system is no longer normal and the eigenvectors are not orthogonal. The lack of orthogonality makes it more difficult to identify and compare modes. In this article these limitations are examined and the impact they have on the results are discussed.

Part II is arranged as follows. In section 2 the transient equations for the dynamics–boundary layer case are derived. In section 3 the methodology is described and the limitations are discussed. Section 4 outlines the process by which modes are compared. Section 5 investigates the differences between the Lorenz and Charney–Phillips grids for capturing the transient modes and notes where limitations on the methodology are relevant. Particular attention is given to the Lorenz grid computational mode. Section 6 offers some closing remarks and motivation for further investigation.

2. Transient equations

As discussed in Part I, the Reynolds-averaged Navier–Stokes (RANS) equations (Tannehill *et al.*, 1997) that simultaneously capture the large-scale dynamics and stably stratified atmospheric boundary layer are

$$\frac{\mathrm{D}u}{\mathrm{D}t} - fv + c_p\theta\frac{\partial\pi}{\partial x} = \frac{1}{\rho}\frac{\partial}{\partial z}\left(\rho\tau_x\right), \tag{1}$$

$$\frac{\mathrm{D}v}{\mathrm{D}t} + fu + c_p\theta\frac{\partial\pi}{\partial y} = \frac{1}{\rho}\frac{\partial}{\partial z}\left(\rho\tau_y\right), \tag{2}$$

$$\frac{\mathrm{D}w}{\mathrm{D}t} + c_p\theta\frac{\partial\pi}{\partial z} = -g, \tag{3}$$

$$\frac{\mathrm{D}\theta}{\mathrm{D}t} = \frac{1}{\rho}\frac{\partial}{\partial z}\left(\rho\mathcal{H}\right), \tag{4}$$

$$\frac{\mathrm{D}\rho}{\mathrm{D}t} + \rho\left(\frac{\partial u}{\partial x} + \frac{\partial v}{\partial y} + \frac{\partial w}{\partial z}\right) = 0, \tag{5}$$

where

$$\frac{\mathrm{D}}{\mathrm{D}t} = \frac{\partial}{\partial t} + u\frac{\partial}{\partial x} + v\frac{\partial}{\partial y} + w\frac{\partial}{\partial z}. \tag{6}$$

A K-closure (Louis, 1979) is used to model the subgrid-scale stress and heat flux terms τ and $\mathcal{H}$; Part I gives details.

Equations (1)–(5) are linearised about the steady-state reference solution constructed in Part I. The reference part is denoted with superscript (r) and superscript $\prime$ is used to denote the transient part. The reference state is the solution to Eqs (25)–(28) in Part I with the boundary conditions described therein. Figures 3 and 4 in Part I show the general reference state flow characteristics.

The coefficients of transient terms are independent of x, y and t, allowing Fourier decomposition with horizontally wavelike solutions $\propto \exp(\mathrm{i}kx + \mathrm{i}ly + \lambda t)$. Here k is the horizontal wavenumber in the x-direction and l is the horizontal wavenumber in the y-direction; $\lambda = \mu - \mathrm{i}\omega$ gives the frequency ω and growth/decay rate μ of the corresponding mode. It is also useful to include the β-effect to prevent degenerate Rossby modes, as described by Thuburn and Woollings (2005). For simplicity, attention is restricted to the $l = 0$ case, i.e. the case for which there is no variation in the y-direction. The constant $\beta = 1.619\times10^{-11}\mathrm{s}^{-1}\mathrm{m}^{-1}$ is used, i.e. a value appropriate to a latitude of 45°N. The full linearised dynamics and boundary-layer equations with $l = 0$ are

$$\lambda u' = -Uiku' - w'\frac{\partial U}{\partial z} + fv' - \frac{\mathrm{i}k\beta}{K^2}u' - c_p\theta^{(\mathrm{r})}\mathrm{i}k\pi' + \frac{1}{\rho^{(\mathrm{r})}}\frac{\partial}{\partial z}\left(\rho^{(\mathrm{r})}\tau_x' + \rho'\tau_x^{(\mathrm{r})}\right) - \frac{\rho'}{\rho^{(\mathrm{r})\,2}}\frac{\partial}{\partial z}\left(\rho^{(\mathrm{r})}\tau_x^{(\mathrm{r})}\right), \tag{7}$$

$$\lambda v' = -Uikv' - w'\frac{\partial V}{\partial z} - fu' - \frac{\mathrm{i}k\beta}{K^2}v' + \frac{1}{\rho^{(\mathrm{r})}}\frac{\partial}{\partial z}\left(\rho^{(\mathrm{r})}\tau_y' + \rho'\tau_y^{(\mathrm{r})}\right) - \frac{\rho'}{\rho^{(\mathrm{r})\,2}}\frac{\partial}{\partial z}\left(\rho^{(\mathrm{r})}\tau_y^{(\mathrm{r})}\right), \tag{8}$$

$$\lambda w' = -Uikw' - \theta'\frac{\partial\pi^{(\mathrm{r})}}{\partial z} - \theta^{(\mathrm{r})}\frac{\partial\pi'}{\partial z}, \tag{9}$$

$$\lambda\theta' = -Uik\theta' - w'\frac{\partial\theta^{(\mathrm{r})}}{\partial z} + \frac{1}{\rho^{(\mathrm{r})}}\frac{\partial}{\partial z}\left(\rho^{(\mathrm{r})}\mathcal{H}' + \rho'\mathcal{H}^{(\mathrm{r})}\right) - \frac{\rho'}{\rho^{(\mathrm{r})\,2}}\frac{\partial}{\partial z}\left(\rho^{(\mathrm{r})}\mathcal{H}^{(\mathrm{r})}\right), \tag{10}$$

$$\lambda\rho' = -Uik\rho' - \rho^{(\mathrm{r})}\mathrm{i}ku' - \frac{\partial}{\partial z}\left(w'\rho^{(\mathrm{r})}\right). \tag{11}$$

With the K-closure, Reynolds stress and heat flux terms are linearised as

$$\tau_x' = K_{\mathrm{m}}'\frac{\partial u^{(\mathrm{r})}}{\partial z} + K_{\mathrm{m}}^{(\mathrm{r})}\frac{\partial u'}{\partial z}, \tag{12}$$

$$\tau_y' = K_{\mathrm{m}}'\frac{\partial v^{(\mathrm{r})}}{\partial z} + K_{\mathrm{m}}^{(\mathrm{r})}\frac{\partial v'}{\partial z}, \tag{13}$$

$$\mathcal{H}' = K_{\mathrm{h}}'\frac{\partial\theta^{(\mathrm{r})}}{\partial z} + K_{\mathrm{h}}^{(\mathrm{r})}\frac{\partial\theta'}{\partial z}. \tag{14}$$

The linearised eddy viscosity K_{m}' and eddy diffusivity K_{h}' are shown in Eq. (15); the square bracketed part of Eq. (15) represents Ri'.

3. Methodology for examining the transients

Equations (7)–(11) can be written in matrix form,

$$\lambda\mathbf{x} = \mathbf{A}\mathbf{x}. \tag{16}$$

The number of solutions (modes) of Eq. (16) depends on the number of degrees of freedom. For the Lorenz grid there are $5n - 1$ degrees of freedom and for the Charney–Phillips grid there are $5n - 2$, where n is the number of vertical levels. Variables stored at the domain boundaries are fixed there. The Lorenz grid stores u, v, θ and ρ together at full model levels while w is stored at half levels; the Charney–Phillips grid differs by storing θ with w at the half levels. The grid arrangement is shown in Figure 1 of Part I. The eigenvector $\mathbf{x}$ describes the vertical spatial structure of each mode and eigenvalues λ describe the temporal structure. Solutions are obtained by performing an eigendecomposition of the matrix $\mathbf{A}$.

For the dynamics-only case with simple reference state and uniform grid examined by Thuburn and Woollings (2005) and Thuburn (2006), it is possible to derive analytically the solution of Eq. (16). The inclusion of the boundary-layer terms and sheared reference state will distort dynamical modes and some may be completely replaced by boundary layer-type modes. The complexity of the coupled equations prevents any analytical description of the dispersion relation

$$K'_{\{\mathrm{m,h}\}} = \frac{l^2}{\left|\frac{\partial \mathbf{u}^{(\mathrm{r})}}{\partial z}\right|}\left(\frac{\partial u^{(\mathrm{r})}}{\partial z}\frac{\partial u'}{\partial z} + \frac{\partial v^{(\mathrm{r})}}{\partial z}\frac{\partial v'}{\partial z}\right) f_{\{\mathrm{m,h}\}}\,(Ri) + l^2\left|\frac{\partial \mathbf{u}^{(\mathrm{r})}}{\partial z}\right|\left.\frac{\partial f_{\{\mathrm{m,h}\}}}{\partial Ri}\right|_{(\mathrm{r})}\left[g\frac{\frac{\partial\left(\frac{\theta'}{\theta^{(\mathrm{r})}}\right)}{\partial z}}{\left|\frac{\partial \mathbf{u}^{(\mathrm{r})}}{\partial z}\right|^2} - 2g\frac{\frac{\partial \ln\theta^{(\mathrm{r})}}{\partial z}}{\left|\frac{\partial \mathbf{u}^{(\mathrm{r})}}{\partial z}\right|^4}\left(\frac{\partial u^{(\mathrm{r})}}{\partial z}\frac{\partial u'}{\partial z} + \frac{\partial v^{(\mathrm{r})}}{\partial z}\frac{\partial v'}{\partial z}\right)\right]. \tag{15}$$

and thus of the total number of each type of mode that will be supported. Instead the spatial and temporal structures of the modes are derived numerically and then carefully examined manually. As in the methodology used for the examination of the steady states in Part I, differences between the Lorenz and Charney–Phillips grid solutions are quantified by comparison against a high-resolution solution. Modes are identified in each low-resolution configuration and then compared against the equivalent mode in the high-resolution solution; the larger number of degrees of freedom in the high resolution means it will capture more modes than the low-resolution cases.

Before continuing with the analysis of the transient part of the system by comparison of the eigenmodes, it is important to consider the type of system for which the mathematical concepts are most suited. Three key features are beneficial: firstly that the system should be normal or normal in a suitable basis (Trefethen and Bau, 1997); secondly that solutions of the continuous equations should exhibit a discrete spectrum (Drazin and Reid, 1984); and thirdly that there should exist a simple relationship between temporal and spatial scales of modes, i.e. the system should have a relatively simple dispersion relation, as in Thuburn and Woollings (2005).

3.1. *Normality*

For the system to be normal it is required that the matrix operator $\mathbf{A}$ satisfies

$$\mathbf{A}^\star\mathbf{A} = \mathbf{A}\mathbf{A}^\star, \tag{17}$$

where $\mathbf{A}^\star$ is the conjugate transpose of $\mathbf{A}$. Whether or not the modes form an orthogonal basis thus depends on the form of the matrix $\mathbf{A}$ and the complexity of the equations it represents.

As discussed above, the dynamics-only case of Thuburn and Woollings (2005) is normal when written in energy variables. This is because the system has a natural measure of the total energy and the total energy of the system is conserved.

The natural measure of total energy in the dynamics-only model is written as

$$E = \frac{1}{2}\mathbf{x}^\star\mathbf{E}\mathbf{x}, \tag{18}$$

where $\mathbf{x}$ is the state vector and $\mathbf{E}$ is a symmetric positive definite matrix of coefficients. The matrix $\mathbf{C} = \mathbf{E}^{1/2}$ can be defined, allowing a change of variables to $\mathbf{y} = \mathbf{C}\mathbf{x}$, which we call energy variables. With this change of variables, the expression of energy simplifies to

$$E = \frac{1}{2}\mathbf{y}^\star\mathbf{I}\mathbf{y}, \tag{19}$$

where $\mathbf{I}$ is the multiplicative identity matrix. The form of the matrix $\mathbf{C}$ is discussed in detail in Holdaway (2010).

If the system conserves energy, then

$$\frac{\mathrm{d}}{\mathrm{d}t}\left(\frac{1}{2}\mathbf{y}^\star\mathbf{y}\right) = 0. \tag{20}$$

Expanding Eq. (20) and using the fact that $\mathrm{d}\mathbf{y}/\mathrm{d}t = \mathbf{B}\mathbf{y}$, where $\mathbf{B} = \mathbf{C}\mathbf{A}\mathbf{C}^{-1}$, gives

$$\begin{aligned}
&\frac{1}{2}\left[\frac{\mathrm{d}\mathbf{y}^\star}{\mathrm{d}t}\mathbf{y} + \mathbf{y}^\star\frac{\mathrm{d}\mathbf{y}}{\mathrm{d}t}\right] &&= 0,\\
\Longrightarrow\ &\frac{1}{2}\left[\mathbf{y}^\star\mathbf{B}^\star\mathbf{y} + \mathbf{y}^\star\mathbf{B}\mathbf{y}\right] &&= 0,\\
\Longrightarrow\ &\frac{1}{2}\left[\mathbf{y}^\star\left(\mathbf{B}^\star + \mathbf{B}\right)\mathbf{y}\right] &&= 0,\\
\Longrightarrow\ &\mathbf{B}^\star = -\mathbf{B}. &&
\end{aligned} \tag{21}$$

If a system has a natural measure of energy, it allows for a simple change of variables to $\mathbf{y}$; if the system also conserves energy then the corresponding operator $\mathbf{B}$ is Hermitian (Eq. (21)) and therefore normal. So, written in the energy variables, the system is normal.

The dynamics-only case is close to normal in the sense that a simple and natural change of basis to energy variables results in eigenmodes that are orthogonal while retaining a straightforward physical interpretation of their structures. If a system is far from normal, then eigenmodes can be made orthogonal only by a rather artificial choice of basis that has no straightforward physical interpretation. If modes are far from orthogonal, then it is possible for multiple modes supported by a particular configuration to have similar structure and there may be certain mode structures captured by one configuration that are not obviously captured by any other configuration. Although the overall linear behaviour is represented by the superposition of far from normal eigenmodes, it is difficult to derive physical interpretation from individual modes and difficult to compare two or more modes between given configurations.

The boundary layer-only model is found to result in a matrix $\mathbf{A}$ that is far from normal and as a result the boundary-layer modes that are captured are difficult to analyse. Coupling to the dynamics brings the operator closer to normal, due to the dynamical modes, which are closer to being orthogonal. The degree of orthogonality between modes in any given configuration is determined by examining the inner product between them.

Writing the system in energy variables will not produce orthogonal eigenmodes since the coupled dynamics–boundary layer model is not energy conserving but dissipates energy. However, writing in energy variables will modify the weighting of the mode structure which is found to help in interpreting mode behaviour. In all subsequent analysis,

energy variables are used and where for example u is plotted it is the u contribution to the energy. Conversion to energy variables involves conversion from density to pressure so the thermodynamic energy variables are θ and p.

Non-normal systems are very common in the physical world and the study of the stability of such systems is possible despite the non-normality (Farrell and Ioannou, 1996, and references therein). Many of the techniques in stability analysis involve the study of the structures that lead to the largest perturbations and these can be examined through use of the singular value decomposition.

3.1.1. *Singular value decomposition*

The singular value decomposition (SVD) was considered as a potential tool for comparing transient linear behaviour between configurations. The SVD, which can be thought of as a generalised eigendecomposition, produces left and right singular vectors and real positive singular values (Trefethen and Bau, 1997). The SVD has the unique property that it always produces orthogonal singular vectors, a potentially useful property in terms of identifying and comparing modes between differing configurations.

Whereas the choice of basis does not impact the physical meaning of eigenvectors, it does impact the singular vectors. Energy variables are chosen since for a dynamics-only case the normality afforded in choosing energy variables would make eigenvectors and singular vectors equivalent. The operator matrix is not positive definite so eigenvalues will be positive and negative, representing eastward and westward propagation; singular values are always positive. For a dynamics-only case, eigenvalues and singular values have equivalent magnitude.

Experiments were performed in order to test whether the SVD would prove a valuable tool for comparison of the coupled case. Physically the singular vectors have structure similar to that seen in the eigenvectors and the overall singular value spectrum is similar to the eigenvalue spectrum. However, there were few examples where the singular vectors were more useful than eigenvectors. They perform well for dynamical-type modes, but no better than the eigendecomposition performs for these modes. For the boundary-layer modes, they also had limited usefulness. Singular vectors with boundary layer-like structure has some unexpected small-scale features, discussed further below.

3.2. *Form of the spectrum*

The set, or spectrum, of eigenvalues λ that the continuous equations supports determines the form of the spectrum. The dynamics-only case, with rigid upper and lower boundaries, has a discrete spectrum of eigenvalues: the wavelike solutions of the continuous equations can have only integer wavenumbers (Thuburn and Woollings, 2005); there is an infinite number of solutions that vary discretely. If the wavelike solutions could have any real wavenumber, there would be an infinite number of solutions that vary continuously, and then the eigenvalue spectrum is said to be continuous.

If the spectrum of solutions is continuous, rather than discrete, there is no guarantee that solutions from different numerical configurations will capture the same modes. It is likely that configurations would sample the spectrum in essentially the same way and over the full range of scales. However, unless the sampling is exactly the same it will make like-for-like comparison difficult or even impossible.

Drazin and Reid (1984) note that all Navier–Stokes flows within a bounded domain exhibit discrete spectra. However, they do not explicitly consider a problem that has linearised boundary-layer terms and viscosity in only a certain region of the domain, as is the case for this coupled dynamics–boundary layer problem. Their results are only suggestive of the kind of spectrum that is expected for the problem being studied here. Some testing has been performed with a small amount of viscosity throughout the domain so as to align the model set-up more closely with that of the Drazin and Reid (1984) case. The inclusion of this viscosity does not appear to alter the overall results and it appears that the spectrum considered here is indeed discrete.

3.3. *Relationship between eigenvalue and eigenvector*

The dynamics-only case has a relatively simple analytical dispersion relation; the spatial scale, determined by integer wavenumber, ranges from the order of the domain size down to infinitely small, in the discrete case limited by the resolution (Thuburn and Woollings, 2005). For each type of mode, the frequency increases or decreases as the scale of the mode decreases, represented by the number of zeros in the mode, shown in Figures 1–4 in Thuburn and Woollings (2005). The result of this simple relationship is that, when using a uniform spacing, a subset of the modes captured by the high-resolution grid will be those modes captured by the low-resolution grid. Depending on how similarly the points are distributed, a high-resolution stretched-grid solution will contain some of the same modes as a low-resolution stretched-grid solution.

If the dispersion relation has a more complex relationship between eigenvalue and eigenvector, then it can make comparison between modes on high- and low-resolution grids more difficult. When a high-resolution boundary layer-only case was examined, all boundary-layer modes had structure that would not be captured by a low-resolution grid. This initial testing implies that all boundary-layer modes contain some small-scale spatial structure that is not obviously related to some large-scale feature. If this is the case, it will likely make it difficult to match up modes in the high- and low-resolution cases.

4. Eigenmode comparison process

Due to the large number of modes, and because of the issues discussed above, it is not a straightforward task to identify and compare modes from each configuration. To focus the study, the number of cases is reduced by considering the steady-state results of Part I. Firstly, given that all configurations that involved averaging of shear resulted in discontinuities in the predicted fields, these configurations need not be considered in the transient part of the comparison. To further limit the study, only the Charney–Phillips grid option I-i is considered here; Part I gives the definitions of all the Charney–Phillips configurations. Option I-i was the most promising overall configuration in terms of the steady state. Therefore, in all reference to Charney–Phillips grid in this section, it is the option I-i configuration that is being considered, unless stated otherwise.

The same experimental framework as in Part I is used. The eigenmode calculation is carried out on coarse-resolution ($n = 10$ levels) and high-resolution ($n = 100$ levels) grids. Choosing a Lorenz grid mode as the starting point, it must be compared with 48 low-resolution Charney–Phillips grid modes, 499 high-resolution Lorenz grid modes and 498 high-resolution Charney–Phillips grid modes. The comparison to both high-resolution grids is essential to ensure the high-resolution modes match, as well as the low-resolution modes. Performing such a comparison by eye is inefficient and so the process is semi-automated by using inner products $\langle \mathbf{x}_1, \mathbf{x}_2 \rangle$ to look for modes in different configurations that are closest to being parallel. For parallel modes,

$$\frac{\langle \mathbf{x}_1, \mathbf{x}_2 \rangle}{\langle \mathbf{x}_1, \mathbf{x}_1 \rangle^{1/2} \langle \mathbf{x}_2, \mathbf{x}_2 \rangle^{1/2}} = 1. \tag{22}$$

The process by which the modes on the Lorenz grid and the modes on the Charney–Phillips grids are compared is summarised as follows:

1. Numerically compute the eigendecomposition of the operator matrix for all the configurations to be compared.
2. Compute the inner product between every Lorenz grid mode and every Charney–Phillips grid mode in the low-resolution configurations to determine the best pairing of modes.
3. Interpolate the low-resolution mode structures to the high-resolution grid and compute the inner product between the low-resolution modes and the high-resolution modes. Also compute inner products between high-resolution configurations.
4. Identify a low-resolution mode that satisfies the following:
   i. It lies in the part of the spectrum of interest;
   ii. The inner product test implies the mode is captured by both low-resolution configurations to be compared;
   iii. The inner product test implies that both high-resolution versions capture the mode and that there is a very close match between high-resolution versions of the mode.
5. Examine the mode structures of the candidates to see if equivalent modes are indeed found and, if not, compare with other modes that the inner product test reports as being close to parallel.
6. If all modes are clearly the same structure and the high-resolution modes are equivalent, then the mode can be used to compare low-resolution configurations.

A certain amount of manual effort is required to point the testing toward the relevant part of the spectrum. Although it is useful to include acoustic modes in the simulation for testing methodology, and given the increasing trend towards fully compressible dynamics in global models, they need not feature in the comparison as results are determined by the dynamics-only studies. The parts of the spectrum of most interest are the inertio-gravity, Rossby and boundary-layer modes and the testing is directed towards them by considering the magnitudes of μ and ω.

5. Transient results

The following presents a comparison of the vertical configurations for the fully coupled dynamics–boundary layer model and an examination of the suitability of the methodology being applied.

As with the steady state, there are a large number of results to draw from and the interested reader is directed to Holdaway (2010) for a more comprehensive presentation. In addition to the five boundary-layer depths considered, there is a degree of choice in the horizontal wavenumber. Thuburn and Woollings (2005) concentrate on a horizontal wavenumber of $k = 2\pi/10^6\ \mathrm{m}^{-1}$ producing a horizontal wavelength of 1000 km. This synoptic-scale structure is large given the relatively shallow depth of the stable boundary layer, so $k = 2\pi/10^3\ \mathrm{m}^{-1}$ is also considered here, giving a 1 km horizontal wavelength.

The comparison of the vertical configurations is ordered as follows: first the Lorenz grid computational mode is examined, second the modes which are deemed to be dynamical type modes are examined and third the modes which are boundary-layer modes are examined.

5.1. *Lorenz grid computational mode*

In the dynamics-only case, the Lorenz grid computational mode can be easily identified in the spectrum since it has zero frequency. In the coupled case, the background flow will act to propagate all modes in an eastward direction. The computational mode, as with all other modes, may only be confidently identified by examining the dominant structure and relating it to the expected physical, or non-physical, properties.

The computational mode is plotted in Figure 1 for the shallowest boundary layer studied in Part I. The structure plotted has the distinct two-grid wave pattern, the dominant field is potential temperature (the quantity being averaged) and the phase speed is approximately given by the reference wind above the boundary layer. For the dynamics-only case, hydrostatic balance results in the two-grid wave contaminating both thermodynamic fields; here geostrophic balance, along with non-resting reference state, above the boundary layer results in contamination of all fields.

Clearly the presence of the boundary layer does not significantly alter the spatial structure of the computational mode, except within the boundary-layer region. The approximate height of the boundary layer in Figure 1 is 100 m; above this height the two-grid wave pattern exists, and below this height the structure is significantly suppressed. Only in the u' and w' fields is structure within the boundary layer significant, however these fields are dominated by the others.

To determine whether suppression of the computational mode in the boundary layer is caused by the boundary-layer diffusion or by the shear in the reference state, the linearised boundary-layer terms are switched off in the transient calculation. Similar suppression of the computational mode is found. Shear in the background flow will propagate waves at different heights at different speeds, disrupting any vertical structure of the form $F(z)\exp(\mathrm{i}kx)$. Waves at higher altitudes effectively catch up with and overtake waves at lower altitudes. This disruption of mode structure by the shear can affect the other dynamical modes

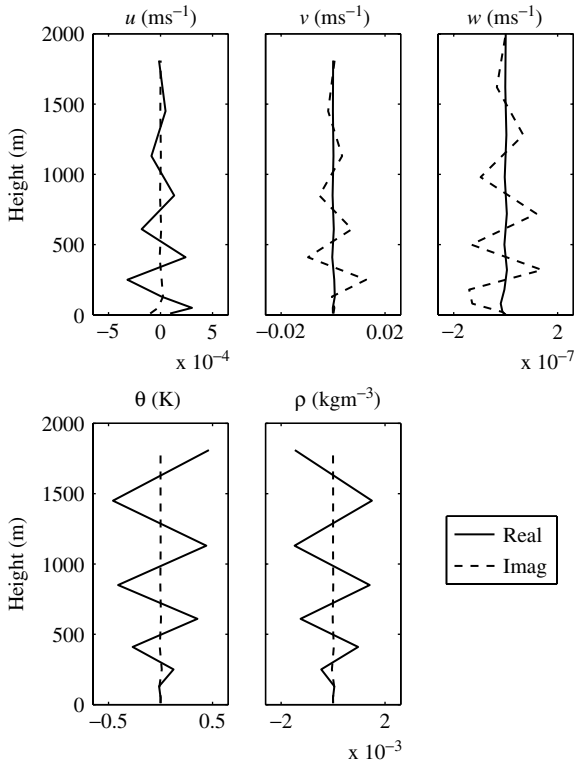

Figure 1. Real and imaginary parts of the Lorenz grid computational mode for the boundary layer 1 background flow with $k = 2\pi/10^6\,\mathrm{m}^{-1}$.

The temporal behaviour of the computational mode is also not altered by the boundary layer. The phase speed is just related to the background flow and the mode remains neutral, i.e μ remains negligible.

Although the mode structure is suppressed in the boundary-layer region, its presence above the boundary layer and the fact that it does not decay in time will cause problems for the Lorenz grid model. Shear appears to suppress the computational mode locally. It is likely an artefact of the methodology that the shear disguises the structure of the mode rather than an indication that shear throughout the domain, as is common in the atmosphere, would mitigate the problems associated with the computational mode. Zhu and Smith (2003) employed a model that has shear throughout the domain but still noted spurious behaviour attributed to the computational mode. Although the shear may disguise the mode structure locally, it is still possible to examine the overall system and gain insight into the types of modes and their behaviour.

5.2. *Comparison of mode frequency*

Figure 2 shows the absolute values of the frequencies of the modes found using the low-resolution Lorenz and Charney–Phillips grids for the $k = 2\pi/10^6\,\mathrm{m}^{-1}$ and boundary layer 1 case. The frequencies, plotted in order of decreasing frequency, correspond only to the modes that are considered to be dynamical modes. Dynamical modes have relatively small decay rate $|\mu|$ and have structures associated with the expected physical behaviour. Generally the mode frequencies appear to be captured equally well, or badly, by the Lorenz and Charney–Phillips grids. Detailed examination of mode structure and comparison to high resolution is required to establish which low-resolution grid produces the most accurate results.

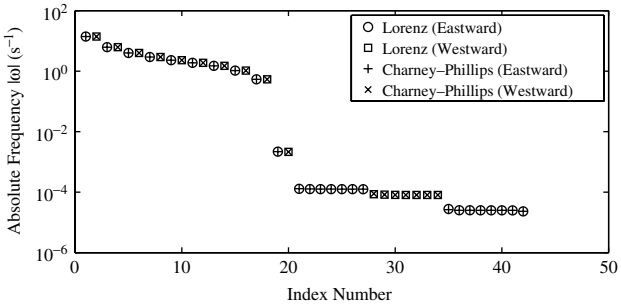

Figure 2. The absolute frequencies $|\omega|$ of the modes found with the low-resolution Lorenz and Charney–Phillips grids. The case is for the boundary layer 1 reference state and horizontal wavelength $k = 2\pi/10^6\,\mathrm{m}^{-1}$. The frequencies of the modes with large enough decay rates to be considered boundary-layer modes are omitted.

Figure 2 is the closest comparison that can be drawn to Figure 1 in Thuburn and Woollings (2005) and Figure 3 in Thuburn (2006), which show the dynamics-only dispersion relations. In Figure 2, both eastward and westward versions of acoustic and inertio-gravity modes are shown; the background flow can cause larger differences between eastward- and westward-propagating pairs than seen in the dynamics-only case.

The highest branch on Figure 2 is the acoustic modes. The two grids capture the frequencies of all the acoustic modes equally well. The two isolated mode frequencies (index 19 and 20) are the external acoustic modes. Throughout the spectrum of acoustic modes, the boundary layer has very little impact on the frequency and structure and so the results do not differ from the dynamics-only case.

The two branches with frequency of the order 10^{-4} are eastward- and westward-propagating inertial modes. Inertial modes refer to inertio-gravity modes that have a very large aspect ratio so that their intrinsic frequency is close to $\pm f$. The structure of all these modes includes the similarity between the u' and v' fields above the boundary layer that is associated with rotating inertial modes. The slower of the middle branches are westward-propagating and remain westward-propagating due to their relative speed of propagation compared to the background wind speed.

The lowest branch in Figure 2 are the Rossby modes and their spatial and temporal behaviour are the most distorted of the dynamical modes. The dominant fields are those associated with Rossby modes and the structure lies primarily between the top of the boundary layer and the top of the domain. Note that the Doppler shifting by the background flow results in all the Rossby modes propagating eastward. Eigenvalues of the Rossby-like modes have a larger magnitude real part than the modes in the middle branch, suggesting an increased level of interaction with the boundary layer.

5.3. *Dynamics–boundary layer interaction*

In order to help gauge how and where the boundary layer interacts with the dynamics, a mode tracking scheme is devised. This is done by adding a multiplication factor to all of the boundary-layer terms in Eqs (7), (8) and (10) that gradually decreases from 1 to 0 in time. When the factor is 0, dynamical modes are computed on a sheared reference state;

as the factor increases and the boundary-layer terms become active, one can track which of these modes are most strongly modified by the boundary layer. The changing behaviour is tracked by computing inner products between modes at subsequent iterations as the factor in the boundary-layer terms is reduced.

The tracking and analysis with the boundary layer off reveals some key factors. The inertio-gravity modes tend to be either inertial modes, i.e. having frequencies around $\pm f$ and structure in the neutrally stratified region above the boundary layer, or gravity modes, i.e. having absolute frequency larger than f and having all their structure in the stably stratified boundary layer. The smooth scale transition seen in Thuburn and Woollings (2005) for a resting, isothermal basic state is not seen. The number of each type, gravity or inertial, depends on the depth of the boundary layer and thus the number of levels within and above the boundary layer. Deeper boundary layers have a larger stratified region in the reference state and so support more gravity modes. Shallow boundary layers have a larger region where Coriolis dominates buoyancy in the reference state and so support more inertial modes.

Boundary-layer modes and gravity modes have similar structure and the tracking reveals that all of the gravity modes obtain some degree of decay as the boundary layer is switched on. With the boundary layer switched on in Eqs (7), (8) and (10), no neutral gravity modes are seen, only boundary-layer, acoustic, inertial and Rossby modes. The number of inertial modes is unchanged as the boundary layer is switched on and their structure is unmodified in the presence of the boundary-layer diffusion. Rossby modes can obtain a decay rate and have their structure strongly modified by the boundary-layer terms. Deeper boundary layers will modify a larger number of Rossby modes than shallow boundary layers and it is the slowest propagating Rossby modes that are first affected.

It is somewhat anticipated that Rossby modes would have greater interaction with the boundary layer than acoustic and inertial modes; acoustic modes propagate very fast and inertial modes will have dominant structure where Coriolis dominates buoyancy, i.e. above the boundary layer and away from the diffusion. In addition it is anticipated that gravity modes would also be damped by the boundary-layer diffusion since in this set-up their structure lies entirely in the boundary-layer region. If the fluid were more strongly stratified above the boundary layer, some neutral gravity modes would likely be found, however this could complicate the analysis further.

5.4. *Dynamical mode structures*

Figures 3 and 4 show an inertial mode and a Rossby mode respectively. The figures show the mode plotted using the energy variable formulation to help determine which are the dominant fields and thus draw physical interpretation. In the lower part of each figure, the spectrum by frequency and growth/decay rate is shown with the location of the plotted mode highlighted.

That Figure 3 represents an inertial mode is clear from the u' and v' dominance and their similarity above the boundary layer. Orthogonality testing reports the modes as being close to parallel to each other across all the configurations and this is confirmed through examination by eye, giving confidence in the comparison. Only the high-resolution Lorenz grid mode is plotted since the Charney–Phillips grid high-resolution mode is sufficiently similar in structure. The overall structure of the mode is captured well by both the Lorenz grid and the Charney–Phillips grid. From the high-resolution mode, one can see how an inertial mode dominates above the boundary layer, where the Coriolis force dominates. In the boundary layer, the mode structure is suppressed as the shear disrupts the vertical waveform, also seen for the computational mode. Note that the structure of the mode bunches up near the top of the boundary layer; this can be explained by a WKB approximation, i.e. vertical wavenumber increases as buoyancy frequency increases, as occurs lower in the domain.

The discontinuity at the top of the boundary layer is not resolved by the low-resolution grids but it is still quite well represented and the velocity does go to zero in the boundary-layer region. The potential temperature field is captured more accurately by the Charney–Phillips grid. It represents the discontinuity well and goes to zero in the boundary-layer region. However potential temperature is not the dominant part of the mode.

As shown in the legend, both low-resolution grids capture the frequency of this eastward-propagating mode well. The decay rate is very small for this dynamical mode, so it is beneficial to accurately capture frequency rather than decay rate for this kind of mode.

Figure 4 shows a Rossby-like mode. The mode is not in the most interesting part of the spectrum, but is found to be closer to being parallel across differing configurations than the more interesting smaller-scale modes. Smaller-scale Rossby-like modes have greater interaction with the boundary layer, causing them to suffer from non-normality. Some small-scale Rossby-like modes also have a *growth* rate, likely a result of an instability associated with the wind shear.

Again the Lorenz grid is compared to the Charney–Phillips grid and the high-resolution solution. This time the Charney–Phillips grid high-resolution solution is shown as well, since there is some discrepancy over mode magnitude in the high resolution. This unfortunately limits the conclusions that can be drawn when comparing the mode at low resolution. Results are similar to those found for the inertial mode, and the general scale and structure of the mode is captured well. As was found for the computational and inertial modes, structure is suppressed in the boundary layer, resulting in a discontinuity that is not well resolved. The high-resolution Lorenz grid is surprisingly poor at resolving this discontinuity and appears to have some two-grid-type structure occurring. Indeed, for some mode components, the low-resolution Charney–Phillips grid appears to produce a more accurate representation near the top of the boundary layer.

The frequency of the mode shown in Figure 4 is well captured by the low-resolution grids when compared to the high-resolution frequency; for this mode μ is very small.

Results presented above are for a shallow boundary layer with large horizontal wavelength. It is clear that results are being limited by the difficulty in finding parallel modes in differing configurations, even in the high-resolution case. The problem is likely a result of non-normality in the system. However, it does seem that configurations are capturing modes that are at least similar to each other.

Different cases of boundary-layer depth have been considered with the smaller horizontal wavelengths. For the modes that could accurately be examined, the findings

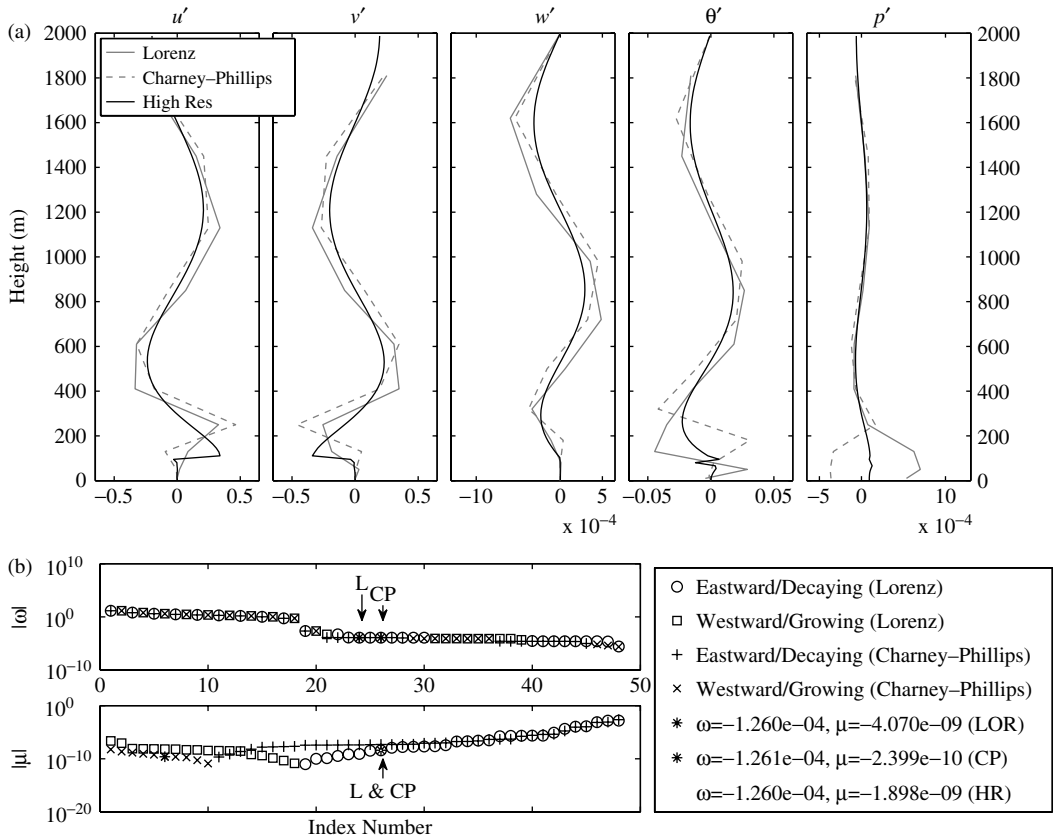

Figure 3. An inertio-gravity mode that is captured by the Lorenz grid, the Charney–Phillips grid and the high-resolution version of the Lorenz grid. The case shown is for boundary layer 1 reference state and horizontal wavenumber $k = 2\pi/10^6 \mathrm{m}^{-1}$. The mode components are plotted by their contribution to the mode energy, i.e. using the energy norm. The plots of μ and ω for the low-resolution configurations are shown in the panel below, with the positions of the plotted modes in the spectrum shown by a $\star$ and an arrow. The values of corresponding μ and ω are given for each case in the lower legend. Note that the two eigenvalue plots are ordered separately and the index numbers do not correspond to one another.

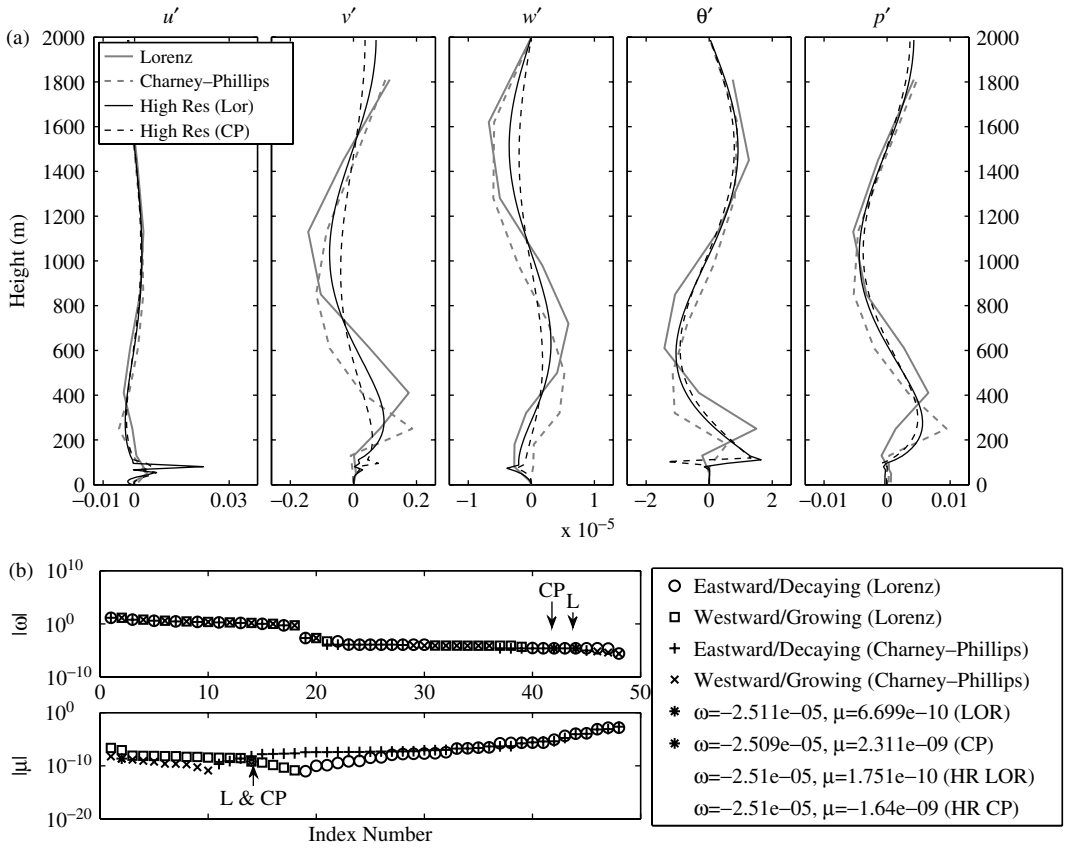

Figure 4. As Figure 3, but for a Rossby-like mode captured by all the grids.

presented above are mostly consistent. The Charney–Phillips grid gives the most accurate representation of the thermodynamic components of the mode and captures the discontinuity near the top of the boundary layer most accurately. The Lorenz grid often performs well for the velocity components but there is generally little to distinguish between the configurations. The biggest issue is that the majority of modes that can be examined lie in the part of the spectrum where differences between the configurations are expected to be small. The more interesting part of the spectrum is where the effects of non-normality are most problematic.

The Charney–Phillips grid is expected to outperform the Lorenz grid for the smallest-scale, slowest-propagating Rossby modes when $k = 2\pi/10^6\mathrm{m}^{-1}$ (Thuburn, 2006). However the majority of these Rossby modes are distorted by the boundary layer and become decaying modes and are hard to examine. That these Rossby modes are so distorted by the boundary layer could potentially mitigate inaccuracy when using the Lorenz grid, since these are the modes that it represents least well. If boundary-layer processes, for which the Lorenz grid is expected to perform well, end up dominating then the Lorenz grid could end up being the preferred grid for modes in this part of the spectrum.

When $k = 2\pi/10^3\mathrm{m}^{-1}$, it is for the inertio-gravity modes, rather than Rossby modes, that the Charney–Phillips grid would be expected to outperform the Lorenz grid (Thuburn, 2006). Since the inertial modes can generally be examined more easily due to their independence from the boundary layer, this configuration would be expected to reveal differences between the Lorenz grid and the Charney–Phillips grid. Figure 5 shows an inertial mode captured by both low- and high-resolution grids; the case is $k = 2\pi/10^3\mathrm{m}^{-1}$ and boundary layer 1.

Given that Figure 5 shows the mode that meets the requirements for comparison most closely, and that there is considerable discrepancy between high-resolution modes, it is clear that the methodology does not perform well for $k = 2\pi/10^3\mathrm{m}^{-1}$. Non-normality in the system is a bigger issue for this case. Also, there are modes with larger growth rates, possibly due to instabilities occurring. Shear-associated instability is expected to be stronger for this wavenumber due to the smaller aspect ratio.

Despite the issues with making a comparison using this case, it does reveal some useful information about the grids. In Figure 5 two-grid wave structure is again seen close to the top of the boundary layer in the high-resolution Lorenz grid solution and is even more pronounced than in previous plots. With a resolution this fine, the solution would be expected to be quite smooth and to capture the structure of the 'truth' mode quite accurately. Instead, some possibly spurious computational mode-like behaviour is occurring that is not present in the high-resolution Charney–Phillips grid solution. Other modes for the short horizontal wavelength case were examined and many modes had this spurious behaviour for the high-resolution Lorenz grid. The two-grid structure could also be an indication of the computational mode contaminating other modes through the non-normality and so be an artefact of the methodology. It represents a rather large disadvantage to using the Lorenz grid if spurious computational mode-type behaviour is present in a number of the modes and so further study in a more simplified system would be warranted.

5.5. *Comparison of boundary-layer modes*

Figure 6 shows the growth and decay rates as found with the Lorenz and Charney–Phillips grids for the $k = 2\pi/10^6\mathrm{m}^{-1}$ and boundary layer 5 case. A deeper boundary layer is chosen as it supports more boundary-layer structure and so can provide higher confidence when establishing whether modes being compared are actually parallel. For a shallow boundary layer, there may only be one low-resolution model level in the boundary-layer region; for deeper boundary layers, there may be up to seven or eight levels in the boundary-layer region.

The modes in Figure 6 that are most physically relevant are those with index between 27 and 33, as these are the slowest damped boundary-layer modes. The modes which have index 31 (Lorenz grid) and 33 (Charney–Phillips grid) are found by the inner product test to be close to parallel to each other. These modes are compared in Figure 7. Both the imaginary and real parts of the mode are plotted since neither part dominates, unlike the dynamical modes. From the figure, it is clear that the inner product test has found the equivalent mode in both low-resolution configurations. However it was not possible, either by eye or using the inner product test, to find a good match in the high-resolution grid for this, or any other, low-resolution pair of modes.

Encouragingly, both Lorenz and Charney–Phillips grids produce similar structures as well as similar decay rates. Other boundary-layer modes were compared and similar agreement was found between the low-resolution configurations elsewhere. However being unable to compare with high-resolution modes prevents a complete investigation from being performed.

That the low- and high-resolution boundary-layer modes are difficult to compare is due to all of the high-resolution boundary-layer modes having structure below the grid scale of the low-resolution grid. For the previously studied dynamics only case, high-resolution solutions would include modes with the same wavenumber as the low-resolution grid solutions. For the boundary-layer modes, the relationship between temporal and spatial scale is more complex and modes with the same approximate scale are not obvious. Even when a high-resolution mode is reported as being almost parallel to an interpolated low-resolution mode, by eye they can look very different. It is possible that the non-normality introduced with the boundary-layer terms is contributing to this more complex relationship between spatial and temporal scale. There is also a near singularity in the formulation of C_m and C_h through the neutral drag coefficient. This, with the very fine resolution near to the surface, could be contributing to small-scale structure near the surface in all of the high-resolution modes.

6. Conclusions

The Lorenz and Charney–Phillips grids have been compared in a model that represents both the linearised large-scale dynamics and the linearised planetary boundary layer. The approach used was to separately compare the ability of the grids to capture the steady state (Part I) and the transients (Part II) of the equation set.

The time-dependent transients of the equations have been compared by considering the eigenmodes of the solution. Examining the modes is a powerful technique that allows individual scales of linear motion to be examined and

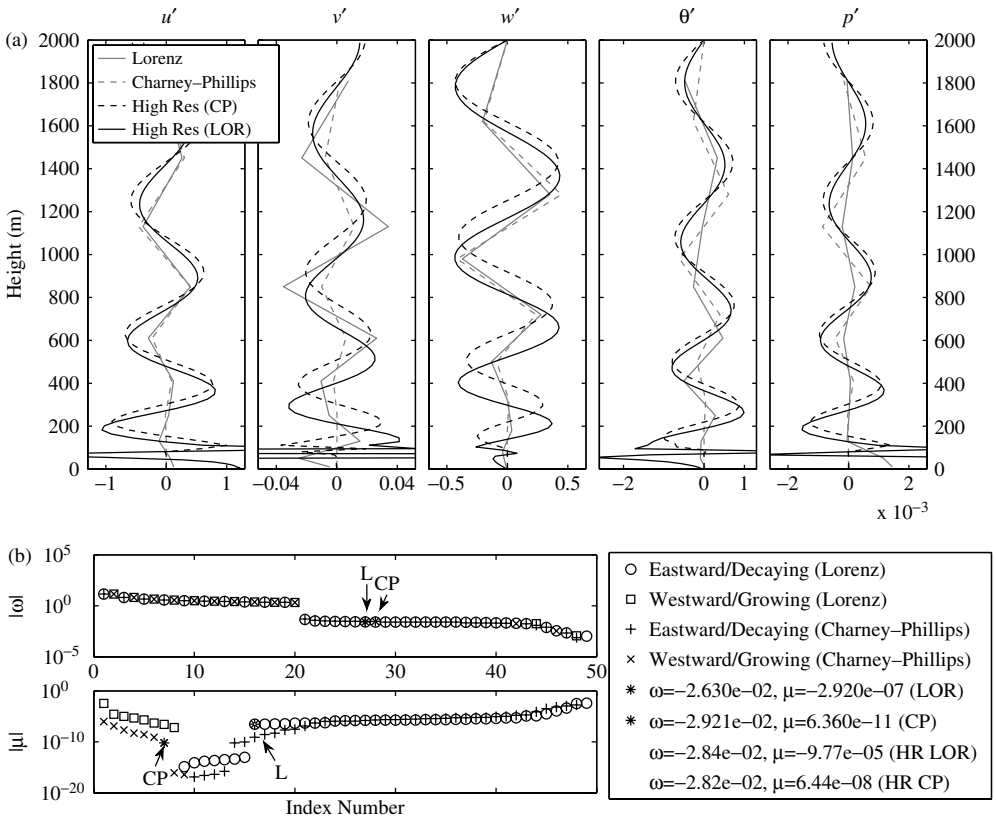

Figure 5. As Figure 4, but for a different inertial mode and found when using the shorter horizontal wavelength $k = 2\pi/10^3 \mathrm{m}^{-1}$.

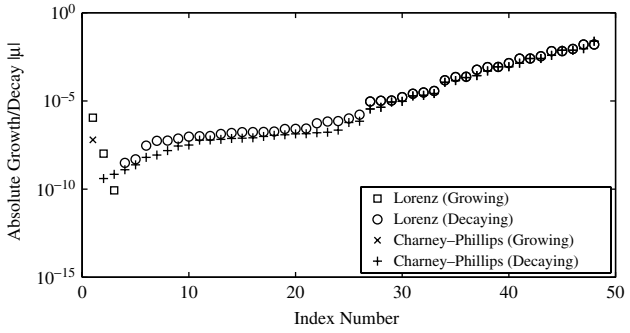

Figure 6. The growth/decay rate μ of the modes as found with the Lorenz grid and the Charney–Phillips grid, for boundary layer 5 reference state and horizontal wavelength $k = 2\pi/10^6 \mathrm{m}^{-1}$.

provides very general results that do not rely on specified initial conditions.

Eigenmode analysis is most useful when the equations exhibit certain mathematical properties, namely that the system is normal, or normal in an appropriate basis, that the spectrum of solutions is discrete, and that there exists a simple relationship between temporal and spatial scale. Boundary-layer processes result in a system which is non-normal and which has a rather complex relationship between scales. Although this has restricted the analysis, a number of interesting results have resulted from the study.

The Lorenz grid computational mode could easily be identified by the two-grid structure and intrinsic zero phase speed in the region of uniform flow. The two-grid wave is heavily suppressed in the boundary-layer region, either by the diffusion or the shear in the reference state, but remains everywhere above the top of the boundary layer. The remaining two-grid structure will be strongly distorted or even removed by the averaging in the vertical momentum equation, resulting in spurious behaviour that can adversely affect the system as a whole.

Two distinct regimes, based upon horizontal wavenumber, were considered when comparing the grids for capturing the dynamical modes. For the large-scale dynamical modes when the horizontal wavenumber is small, so the aspect ratio is large, both grids perform well and are capable of accurately capturing the mode structures. Gravity modes and the slowest propagating Rossby modes are found to be the dynamical modes most strongly modified by the boundary-layer diffusion. That the slowest Rossby modes decay partially mitigates a disadvantage of the Lorenz grid, since it is less accurate than the Charney–Phillips grid for slow Rossby modes with large horizontal wavelength (Thuburn and Woollings, 2005).

For inertial modes with small horizontal wavenumber and large aspect ratio, both Lorenz and Charney–Phillips grids capture the temporal and spatial structure well. When the aspect ratio is small, a discrepancy is anticipated between the ability of the Lorenz and Chareny–Phillips grids for inertial modes, which are not generally modified by the boundary layer. It would be useful to measure the extent of the discrepancy when the boundary layer is included. However, the smaller aspect ratio contributes to non-normality. This added difficulty prevented a useful comparison of the inertial modes in this wavenumber regime.

When modes were examined for the larger horizontal wavenumber case, some unexpected behaviour in the Lorenz grid configurations was revealed. The high-resolution solution supports some grid-scale features where there are discontinuities in the mode at the top of the boundary layer. High-resolution solutions would be expected to be smooth

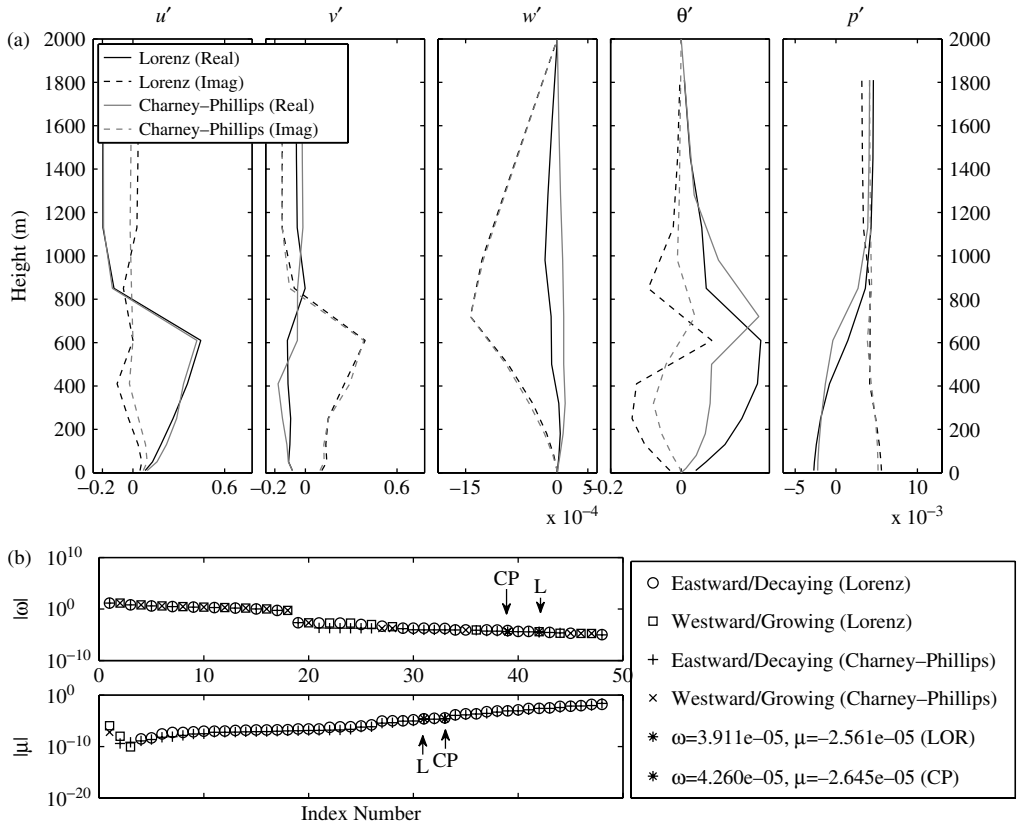

Figure 7. As Figures 3–5, but for a boundary layer mode, with boundary layer 5 reference state and horizontal wavelength $k = 2\pi/10^6 \mathrm{m}^{-1}$. No high-resolution mode is plotted and both real and imaginary parts of the mode are shown.

and close to the 'truth' mode. This could be pointing to a wider issue related to using the Lorenz grid on a stretched grid, or for a flow with vertical discontinuity, and would warrant further investigation.

Comparison of boundary-layer modes was most problematic, due to the non-normality and apparent complex scale relationship induced by the presence of the linearised diffusion coefficients. Although low-resolution boundary-layer modes could be compared between configurations, it was impossible to identify the corresponding high-resolution mode. All high-resolution boundary-layer modes have structure that is below the grid scale of the low-resolution grid.

Acknowledgements

The lead author wishes to thank the EPSRC and the Met Office for funding this work under an Industrial CASE partnership. Further thanks are due to the dynamics research group at the Met Office for providing access to their expertise.

References

Arakawa A, Konor CS. 1996. Vertical differencing of the primitive equations based on the Charney–Phillips grid in hybrid $\sigma - p$ vertical coordinates. *Mon. Weather Rev.* **124**: 511–528.

Charney JG, Phillips NA. 1953. Numerical integration of the quasi-geostrophic equations for barotropic and simple baroclinic flows. *J. Meteorol.* **10**: 71–99.

Drazin PG, Reid WH. 1984. *Hydrodynamic Stability*. Batchelor GK, Miles JW. (eds) Cambridge University Press: Cambridge, UK.

Farrell BF, Ioannou PJ. 1996. Generalized stability theory. Part I: Autonomous operators. *J. Atmos. Sci.* **53**: 2025–2040.

Fox-Rabinovitz MS. 1994. Computational dispersion properties of vertically staggered grids for atmospheric models. *Mon. Weather Rev.* **122**: 377–392.

Garrett JR. 1992. *The Atmospheric Boundary Layer*. Cambridge University Press: Cambridge, UK.

Holdaway D. 2010. 'Coupling the planetary boundary layer to the large-scale dynamics of the atmosphere: The impact of vertical discretisation'. PhD thesis. University of Exeter: UK.

Holdaway D, Thuburn J, Wood N. 2012. Comparison of Lorenz and Charney–Phillips vertical discretisations for dynamics–boundary layer coupling. Part I: Steady states. *Q. J. R. Meteorol. Soc.* DOI: 10.1002/qj.2016.

Holton JR. 2004. *An Introduction to Dynamic Meteorology*. *Internat. Geophys. Series* **88**: Elsevier Academic Press.

Kalnay E. 2003. *Atmospheric Modeling, Data Assimilation and Predictability*. Cambridge University Press: Cambridge, UK.

Lauritzen PH, Jablonowski C, Taylor MA, Nair RD. (eds) 2011. *Numerical Techniques for Global Atmospheric Models*. Springer: Berlin.

Leslie LM, Purser RJ. 1992. A comparative study of the performance of various vertical discretization schemes. *Meteorol. Atmos. Phys.* **50**: 61–73.

Lorenz EN. 1960. Energy and numerical weather prediction. *Tellus* **12**: 364–373.

Louis J-F. 1979. A parametric model of vertical eddy fluxes in the atmosphere. *Boundary-Layer Meteorol.* **17**: 187–202.

Stull RB. 1988. *An Introduction to Boundary-Layer Meteorology*. Kluwer Academic Publishers.

Tannehill JC, Anderson DA, Pletcher RH. 1997. *Computational Fluid Mechanics and Heat Transfer*. Taylor and Francis.

Thuburn J. 2006. Vertical discretizations giving optimal representation of normal modes: Sensitivity to the form of the pressure-gradient term. *Q. J. R. Meteorol. Soc.* **132**: 2809–2825.

Thuburn J, Woollings T. 2005. Vertical discretizations for compressible Euler equation atmospheric models giving optimal representation of normal modes. *J. Comput. Phys.* **203**: 386–404.

Trefethen LN, Bau D. 1997. *Numerical Linear Algebra*. SIAM: Philadelphia, USA.

Zhu H, Smith RK. 2003. Effects of vertical differencing in a minimal hurricane model. *Q. J. R. Meteorol. Soc.* **129**: 1051–1069.

